What is the skill of ocean tracers in reducing uncertainties about ocean diapycnal mixing and projections of the Atlantic Meridional Overturning Circulation?

Marlos Goes,[1] Nathan M. Urban,[1] Roman Tonkonojenkov,[1] Murali Haran,[2] Andreas Schmittner,[3] and Klaus Keller[1,4]

Received 26 May 2010; revised 30 July 2010; accepted 25 August 2010; published XX Month 2010.

[1] Current projections of the oceanic response to anthropogenic climate forcings are uncertain. Two key sources of these uncertainties are (1) structural errors in current Earth system models and (2) imperfect knowledge of model parameters. Ocean tracer observations have the potential to reduce these uncertainties. Previous studies typically consider each tracer separately, neglect potentially important statistical properties of the system, or use methods that impose rather daunting computational demands. Here we extend and improve upon a recently developed approach using horizontally averaged vertical profiles of chlorofluorocarbon (CFC-11), radiocarbon ($\Delta^{14}C$), and temperature (T) observations to reduce model parametric and structural uncertainties. Our method estimates a joint probability density function, which considers cross-tracer correlations and spatial autocorrelations of the errors. We illustrate this method by estimating two model parameters related to the vertical diffusivity, the background vertical diffusivity, and the upper Southern Ocean mixing. We show that enhancing the upper Southern Ocean mixing in the model improves the representations of ocean tracers and improves the hindcasts of the Atlantic Meridional Overturning Circulation (AMOC). The most probable value of the background vertical diffusivity in the pelagic pycnocline is between 0.1 and 0.2 cm^2 s^{-1}. According to the statistical method, observations of $\Delta^{14}C$ reduce the uncertainty about the background vertical diffusivity mostly followed by CFC-11 and T. Using all three tracers jointly reduces the model uncertainty by 40%, more than each tracer individually. Given several important caveats, we illustrate how the reduced model parametric uncertainty improves probabilistic projections of the AMOC.

Citation: Goes, M., N. M. Urban, R. Tonkonojenkov, M. Haran, A. Schmittner, and K. Keller (2010), What is the skill of ocean tracers in reducing uncertainties about ocean diapycnal mixing and projections of the Atlantic Meridional Overturning Circulation?, *J. Geophys. Res.*, *115*, XXXXXX, doi:10.1029/2010JC006407.

1. Introduction

[2] The North Atlantic Overturning Circulation (AMOC) is a key component of the climate system [*Munk and Wunsch*, 1998]. Past changes in the AMOC intensity are associated with considerable changes in global scale temperature and precipitation patterns [*McManus et al.*, 2004]. Anthropogenic climate forcings may trigger an AMOC threshold response, with potentially serious impacts on natural systems and human welfare [*Patwardhan et al.*, 2007; *Keller et al.*, 2000]. Current AMOC model predictions are deeply uncertain [*Zickfeld et al.*, 2007; *Meehl et al.*, 2007].

[3] Tracer observations such as chlorofluorocarbon-11 (CFC-11) and radiocarbon ($\Delta^{14}C$) provide information on the ventilation rate and advective properties in the ocean on time scales ranging from decadal to centennial that can be used for evaluating the skill of climate models in simulating the ocean circulation [*Doney et al.*, 2004]. A better representation of these processes in models can possibly improve AMOC projections.

[4] A key variable for determining ocean circulation properties in models is the vertical ocean diffusivity (K_v). Changing this value in model simulations has a large impact on oceanic heat storage and transport, uptake of ocean tracers such as CO_2 [*Sokolov et al.*, 1998], and on the work necessary to lift the abyssal waters through stratification (that closes the MOC circulation) [*Wunsch and Ferrari*,

[1]Department of Geosciences, Pennsylvania State University, University Park, Pennsylvania, USA.
[2]Department of Statistics, Pennsylvania State University, University Park, Pennsylvania, USA.
[3]College of Oceanic and Atmospheric Sciences, Oregon State University, Corvallis, Oregon, USA.
[4]Earth and Environmental Systems Institute, Pennsylvania State University, University Park, Pennsylvania, USA.

0148-0227/10/2010JC006407

2004]. This variable is highly uncertain [*Munk and Wunsch*, 1998], and it is sometimes tuned in models to generate a realistic AMOC strength [*Gao et al.*, 2003]. In addition, this parameter value affects the existence of multiple states of the MOC in model simulations [*Schmittner and Weaver*, 2001].

[5] Various processes lead to mixing in the ocean such as shear or buoyancy forced turbulence, interactions of flow with topography, and double diffusion (differential molecular diffusion of heat and salt). See *Smyth and Moum* [2001] and *Moum and Smyth* [2001] for reviews. Although General Circulation Models have been increasing their ability of parameterizing subgrid scale turbulent processes in the ocean [*Bryan and Lewis*, 1979; *Pacanowski and Philander*, 1981; *Large et al.*, 2004; *Ferrari et al.*, 2008], due to the complexity of the problem and processes involved, most schemes are still highly simplified and parameterized. In Earth System Models of Intermediate Complexity (EMICs), the absence of more complex parameterizations elevates the importance of the parameters related to K_v in order to fulfill the model necessity of turbulent mixing in simulating a realistic AMOC strength.

[6] Several studies [e.g., *England*, 1993; *Gao et al.*, 2003] analyze the importance of the magnitude of the diffusivity strength and parameterization on the MOC structure and representations of tracers in ocean models. These studies are typically silent on the question of how much information is contained in the different types of observations. This is an important question, for example, to inform the design of AMOC observation and prediction systems [cf. *Baehr et al.*, 2008; *Keller et al.*, 2007].

[7] *Schmittner et al.* [2009] discusses a relatively simple but computationally efficient method to estimate the background ocean diffusivity K_{bg} from the combination of spatially resolved ocean tracer observations considering both, observational and model errors. However, *Schmittner et al.* [2009] neglects the effects of cross correlation between different tracers, which limits the number of tracers that can be combined in a joined probability density function. In another recent study, *Bhat et al.* [2009] estimates the posterior probability distribution for K_{bg} using Δ^{14}C and CFC-11 observations. Their approach uses a Gaussian process emulator for the climate model and estimates the distribution of K_{bg} via a Bayesian approach. While their kernel mixing based approach to constructing the emulator is flexible and efficient, it is conceptually complex and computationally highly demanding for routine use with more than two ocean tracers.

[8] Here we estimate the probability density function (pdf) of K_{bg} using three tracers simultaneously. Our approach provides a fast and easy way to implement the methodology, enabling the routine use of information from several ocean tracers jointly, while still considering spatial autocorrelation as well as cross correlation between residuals of different tracers. We demonstrate how neglecting cross correlation and/or simplifying the mean function can compromise the accuracy of the estimation. We improve the treatment of uncertainties surrounding K_v in the model by considering the structural uncertainty about the upper Southern Ocean mixing (u_K_{SO}). We show that an ensemble with enhanced Southern Ocean mixing is more consistent with the observations.

[9] Furthermore, we advance on previous work by quantifying and ranking the skill of the tracers CFC-11, Δ^{14}C and temperature (T) to constrain the uncertainties in the model parameter K_{bg}. We demonstrate the potential utility of the considered observations to improve model predictions of the AMOC.

2. Methods

2.1. Earth System Model of Intermediate Complexity

[10] We use the University of Victoria Earth System Model of Intermediate Complexity (UVic 2.8) [*Weaver et al.*, 2001]. This model has been widely used in climate simulations and models comparisons studies. In the UVic model, we parameterize the diapycnal diffusivity as $K_v = K_{tidal} + K_{SO} + K_{bg}$, which consists of the diffusivity due to local dissipation of tidal energy and its resulting generation of turbulence and mixing (K_{tidal}) [*Simmons et al.*, 2004], a parameterization for the vigorous mixing (K_{SO}) observed in the Southern Ocean [e.g., *Naveira Garabato et al.*, 2004], plus a background diffusivity K_{bg} that represents all other processes that lead to mixing, such as nonlocal dissipation of tidal energy, mesoscale eddy activity, double diffusion, hurricanes, interaction of flow with topography, and others.

[11] The model accounts for increased mixing over rough topography based on the tidal mixing scheme of *St. Laurent et al.* [2002], and uses the [*Gent and McWilliams*, 1990] eddy mixing parameterization. It is likely that K_{bg} is spatially and temporally variable in nature [*Sriver et al.*, 2010], but due to a lack of a more explicit representation of the processes and for simplicity we assume a constant value of K_{bg} everywhere. Note that K_{tidal} decays exponentially (with an *e*-folding depth of 500 m above the seafloor) such that it is unimportant in the pelagic pycnocline (i.e., away from the boundaries). However, it is the value of K_{bg} in the pelagic pycnocline that is most important in determining the large-scale ocean circulation in models [cf., *Marotzke*, 1997; *Munk and Wunsch*, 1998]. For the Southern Ocean (south of 40S) parameterization, the vertical mixing is truncated at 1 cm^2/s as a lower bound ($K_v > 1$ cm^2/s). The Southern Ocean is one of the most tempestuous oceans on Earth, and these transient effects may produce strong turbulent mixing, specially in the upper Southern Ocean. In order to include uncertainties about the upper Southern Ocean mixing, we further divide the Southern Ocean mixing into upper (u_K_{SO}) and lower (l_K_{SO}) parts. Therefore, $K_{SO} = u\_K_{SO} + l\_K_{SO}$, where u_K_{SO} is the Southern Ocean mixing in the upper 500 m, and l_K_{SO} is the Southern Ocean mixing from 500m to the bottom of the water column.

[12] We create two ensembles to analyze the uncertainty in two model parameters, the background ocean diffusivity (K_{bg}) and the upper Southern Ocean diffusivity (u_K_{SO}). Each ensemble contains seven members, corresponding to a grid of the parameter K_{bg} values of (0.05, 0.1, 0.15, 0.2, 0.3, 0.4, and 0.5) cm^2 s^{-1}. The difference between the two ensembles is that in the first one (ENSEMBLE 1), the enhanced SO mixing is only applied in the lower part of the Southern Ocean, so in the upper SO the mixing is equal to the rest of the pelagic areas of the upper ocean (with indices $u\_K_{SO} = 0$, $l\_K_{SO} = 1$), whereas the second one (ENSEMBLE 2) uses an enhanced mixing in the entire column of the Southern Ocean (with indices $u\_K_{SO} = 1$, $l\_K_{SO} = 1$). As we

are not varying the parameter l_K_{SO}, it is suppressed in the rest of the manuscript.

[13] The ocean component in UVic is MOM2 [*Pacanowski*, 1995] with a 1.8° × 3.6° resolution in the horizontal and 19 depth levels. The atmospheric component is a one-layer atmospheric energy-moisture balance model, which does not apply flux correction and is forced by prescribed winds from the NCAR/NCEP climatology. Also included in the model are a thermodynamic sea ice component, a terrestrial vegetation (TRIFFID), and an oceanic biogeochemistry based on the ecosystem model of *Schmittner et al.* [2005].

[14] A total of 47,600 model years was preformed, what makes UVic suitable for this kind of study. At first, the model is spun up from observed data fields as initial conditions for 3000 years (with a coupled carbon cycle for the last 1000 years) for each parameter value. It is then integrated from years 1800–2100 using historical and projected climate forcings (SRES-A1FI scenario), extended to the year 2200 following [*Zickfeld et al.*, 2008]. We modify the model to include non-CO_2 greenhouse gases, volcanic and sulfate forcings from *Sato et al.* [1993] and *Hansen and Sato* [2004]. Atmospheric sulfates data enter the model as gridded optical depth [*Koch et al.*, 1999], and follow the same rate of decrease as the CO_2 concentration after 2100.

2.2. Data

[15] We focus on a subset of observations that have previously been shown to provide constraints on the parameterization of K_v in ocean models: (1) temperature (T), (2) chlorofluorocarbon 11 (CFC-11), and (3) radiocarbon (Δ^{14}C) observations [cf. *Schmittner et al.*, 2009; *Bhat et al.*, 2009; *Toggweiler et al.*, 1989]. Δ^{14}C is defined as the ^{14}C/^{12}C ratio of air-sea fractionation-corrected data [*Stuiver and Polach*, 1977]. Each of the tracers in this subset has a different behavior and can constrain K_v in different ways. The temperature observations constrain K_v, because K_v affects, for example, the shape of the thermocline as well as the penetration of the anthropogenic heat anomalies [*Gnanadesikan*, 1999]. The Δ^{14}C observations can constrain K_v in two main ways, because it has a natural and an anthropogenic component. The natural component can provide information of mixing rates (that are, in turn, a function of K_v) in the order of centuries or millennia. The anthropogenic component, which greatly increased during the 1950s and 1960s due to thermonuclear explosions, provides information on decadal time scale. Here we do not make distinction between natural and bomb ^{14}C, thus we use its total concentration. The anthropogenic tracer CFC-11 also constrains K_v on decadal time scale, because atmospheric emissions started in the 1930s. The solubility of CFCs in water is dependent on the temperature. Considering CFC-11 and Δ^{14}C jointly can provide new insights into vertical oceanic mixing because they have very different forcing histories, air-sea equilibration time scales and water solubility [*Broecker and Peng*, 1987; *Ito et al.*, 2004], and the observation errors and signal-to-noise ratios of the two tracers are different. We analyze published data products for these three tracers [*Locarnini et al.*, 2006; *Key et al.*, 2004] and average the model hindcasts over the time the observations have been collected, i.e., 1990s for CFC-11 and Δ^{14}C, and 1950–2000 for temperature. We interpolate the observations to the model grid and the model output is restricted to the regions where the data products are available. All considered ocean tracer observations are horizontally averaged into global mean vertical profiles. Further, the probability distributions of the model parameters, inferred from the information of ocean tracers profiles, are compared with the distribution inferred from the climatological observations of the AMOC strength at 24°N. For this purpose, we use the information of the AMOC strength calculated with the inverse model of *Lumpkin and Speer* [2003], which is estimated as (17.6 ± 2.7 Sv). The model ensembles are calibrated against observations using a Bayesian inference method. We assume a Gaussian likelihood function and estimate the posterior probability of K_{bg} and u_K_{SO} given the observations through a Markov Chain Monte Carlo (MCMC) method [*Metropolis et al.*, 1953]. Our method accounts for autocorrelations of the residuals, as well as cross correlation between residuals of different tracers. For this, a separable covariance matrix Σ is estimated. The inversion and the numerical implementation of the calibration procedure are detailed in the next subsection. Readers not interested in the details of the statistical inversion technique can skip the next subsection without loss of understanding.

2.3. Bayesian Model Inversion

[16] The goal of Bayesian parameter estimation is to infer a probability distribution(s) $p(\theta\,|O)$ representing the uncertainty in one (or more) climate model parameter θ, conditional on a vector of observed data O. Here θ are parameters K_{bg} and u_K_{SO}, which are related to the vertical ocean diffusivity in UVic. The inferential procedure is based on a statistical model that relates the model parameters (θ) to the observations (O) by way of the ensemble of model output $M(\theta)$. The statistical model used here assumes that the observations are randomly distributed around the model prediction, according to

$$O = M(\theta) + \epsilon, \tag{1}$$

where the error is a random variable drawn from a multivariate normal distribution

$$\epsilon \sim N(\mu, \Sigma), \tag{2}$$

with an unknown mean or bias term μ and covariance matrix Σ. These distributional parameters are estimated along with the model parameter θ. The error term encompasses all processes which may cause the observations to deviate from the model predictions, including model structural error, unresolved variability in the climate system, and measurement error. We model these errors as random processes, approximated here by a potentially correlated Gaussian probability function.

[17] The error mean term μ represents model bias, which is common for each observed variable across ensemble members. *Schmittner et al.* [2009] assumed a bias which is constant with depth. Here we expand upon this form by using a general linear form that varies with depth (z), $\mu = az + b$. This form improves the model fit as indicated by a exploratory data analysis in the next section. The covariance matrix, described later, captures the residual variability that is unaccounted by the linear bias term.

[18] The above probability model describing the spread of observations about the model output defines a likelihood function $L(O|\theta, \mu, \Sigma)$ for the data conditional on the model and covariance parameters

$$L(O|\theta,\mu,\Sigma) = (2\pi)^{-N/2}|\Sigma|^{-1/2}\exp\left(-\frac{1}{2}\tilde{r}^T\Sigma^{-1}\tilde{r}\right), \quad (3)$$

where Σ is a covariance matrix and $\tilde{r} = O - M(\theta) - \mu$ are the bias-corrected data-model residuals.

[19] Consider an ensemble M containing p runs of a climate model, where each run corresponds to a different value of a climate model parameter, θ_k, $k = 1, \ldots, p$. For each ensemble member we analyze n ocean tracer profiles defined at d spatial locations (depths). The matrix Σ is $nd \times nd$ specifying the covariance between n tracers at d locations (depths). Assuming separability, Σ can be approximated by a Kronecker product of two matrices

$$\Sigma = \Sigma_T \otimes C_S + \Sigma_M, \quad (4)$$

where Σ_T corresponds to the $n \times n$ cross-covariance matrix of the tracers, and C_S is the $d \times d$ spatial correlation matrix (in depth) respectively. Σ_M is the data measurement error which we assume to be negligible compared to the other errors because of the spatial aggregation of the data.

[20] The cross-covariance matrix Σ_T depends on $n(n-1)/2$ cross-tracer correlation coefficients ρ_{ij} (since $\rho_{ij} = \rho_{ji}$), and on residual standard deviations σ_i of the n individual tracers

$$\Sigma_T = \begin{bmatrix} \sigma_1^2 & \sigma_1\sigma_2\rho_{12} & \ldots & \sigma_1\sigma_n\rho_{1n} \\ \sigma_2\sigma_1\rho_{21} & \sigma_2^2 & \ldots & \sigma_2\sigma_n\rho_{2n} \\ \vdots & \vdots & \ddots & \vdots \\ \sigma_n\sigma_1\rho_{n1} & \ldots & \ldots & \sigma_n^2 \end{bmatrix}. \quad (5)$$

[21] We model the spatial correlation C_S using a Gaussian correlation function, a special case of the Matérn class of covariance functions (see, for e.g., *Stein* [1999]). This function decays with distance between locations d_i and d_j with a correlation length scale λ, assumed to be the same for all tracers

$$(C_S)_{ij} = \exp\left(-\frac{|d_i - d_j|^2}{\lambda^2}\right). \quad (6)$$

[22] Given the property of the Kronecker product (see, for example, *Lu and Zimmerman* [2005]), the multivariate normal likelihood function $L(y, \theta)$ becomes

$$L(O|\theta,\mu,\Sigma_T,C_S) = (2\pi)^{-N/2}\left(|\Sigma_T|^d|C_S|^n\right)^{-1/2} \cdot \exp\left[-\frac{1}{2}\tilde{r}^T\left(\Sigma_T^{-1}\otimes C_S^{-1}\right)\tilde{r}\right], \quad (7)$$

where $N = nd$ is the total number of data points, and $\tilde{r} = [O_1 - M_1 - \mu_1, \ldots, O_n - M_n - \mu_n]^T$ is the concatenated vector containing the misfit between the unbiased model predictions and the corresponding observations for the considered tracers. The Kronecker structure of equation (4) allows the $nd \times nd$ matrix Σ to be efficiently inverted by inverting the two smaller matrices Σ_T $(n \times n)$ and C_S $(d \times d)$.

[23] Once the probability model has been specified in the form of a likelihood function, the Bayes' theorem allows inference about the posterior distribution of θ. The theorem states that the posterior probability of the unknown parameters is proportional to their prior probability distribution, multiplied by the likelihood of the data, according to

$$p(\theta,a,b,\sigma,\rho,\lambda|O) \propto L(O|\theta,a,b,\sigma,\rho,\lambda)p(\theta)p(a) \cdot p(b)p(\sigma)p(\rho)p(\lambda). \quad (8)$$

We draw 20,000 samples from the above posterior distribution by a Markov chain Monte Carlo (MCMC) algorithm. The MCMC algorithm jointly estimates the model parameters ($\theta = K_{bg}$, u_K_{SO}), $2n$ bias coefficients (a_i and b_i), n standard deviations (σ_i), $n(n-1)/2$ cross-tracer correlations (ρ_{ij}), and one correlation length (λ). This is an improvement upon the methodology of *Schmittner et al.* [2009] which held all parameters but θ fixed at optimized values, and did not consider the uncertainty in the other parameters. Because the model output is only defined on a discrete grid of values, the MCMC algorithm proposes discrete jumps for the parameters θ during its random walk through parameter space, and continuous moves for all other parameters.

[24] We choose a uniform prior $p(\theta)$ for the model parameters K_{bg} and u_K_{SO}. For the correlation length we apply the lognormal prior $\ln \lambda \sim N(5.5, 0.5^2)$, such that the logarithm of λ is normally distributed with mean 5.5 and standard deviation 0.5. This prior locates most of the probability mass of the distribution between 0 and 600 meters. We use normal priors for the bias parameters a_i and b_i, $p(a_i) = N(0, (\sigma_i/\lambda)^2)$ and $p(b_i) = N(0,\sigma_i^2)$. For the estimate of individual tracers distributions, where the cross-correlation matrix is a scalar (i.e., $\Sigma = \sigma_1^2$), we use a Jeffreys prior ($p(\sigma_i) \propto 1/\Sigma$). When the multitracer cross-covariance matrix is estimated, we specify an inverse Wishart prior distribution $\Sigma_T \sim IW(S, \nu)$, with a diagonal scale matrix $S = I$ and $\nu = 2n + 1$ degrees of freedom. A diagonal scale matrix reduces spurious correlations by penalizing tracer residuals which are not independent of each other. Spurious correlation is not a problem when the data dimension is large, but when the data are sparse such a regularization procedure is prudent (see, for instance, *Barnard et al.* [2000] or Chapter 19 of *Gelman et al.* [2003], and references therein).

[25] Equation (8) provides the joint posterior probability of both the model parameter and the bias and covariance parameters. The marginal posterior probability of the model parameter alone is obtained by integrating the joint posterior over all other parameters,

$$p(\theta|O) = \int p(\theta,a,b,\sigma,\rho,\lambda|O)\,da\,db\,d\sigma\,d\rho\,d\lambda. \quad (9)$$

[26] Since the posterior is estimated by MCMC sampling, this posterior distribution of θ is easily obtained by simply

considering the θ samples while ignoring the samples for the other parameters.

3. Results

3.1. Effect of Ocean Diapynal Diffusivity on the AMOC Hindcasts and Spatial Fields

[27] In the adopted model the AMOC strength is positively correlated with the parameters K_{bg} and u_K_{SO} (Figure 1). K_{bg} has a strong influence on the model hindcasts of the maximum AMOC strength, while the AMOC sensitivity to u_K_{SO} is weaker. The range of AMOC strength varies from about 5–23 Sv across all simulations. The inclusion of enhanced upper Southern Ocean mixing (u_K_{SO} = 1), can increase the AMOC by a few Sverdrups, with more influence at lower K_{bg}. Under the projected climate forcings, the AMOC strength decreases in most cases, but it is more sensitive (in absolute values) to the considered forcings for higher diffusivity values. Due to the strong dependence of the AMOC structure and behavior on the values of the parameters K_{bg} and u_K_{SO} in this model, a reduction in the parametric uncertainty has the potential to improve AMOC hindcast and projection in the model.

[28] The different parameter values result in different hindcasts of ocean tracers such as CFC-11 (Figure 2) and Δ^{14}C (Figure 3), due to the different tracers advection and diffusion rates in the model. Higher K_{bg} values result in stronger vertical water exchange, increased deep water mass formation, which carries water with higher tracer content from the surface, and decreased vertical stratification in the ocean. u_K_{SO} broadly produces the same effects of K_{bg}. Nevertheless, u_K_{SO} impacts more heavily the lower K_{bg} runs and the Southern Ocean stratification.

[29] Here we analyze the tracers concentrations as vertical profiles of their averaged concentrations over the globe. We consider three different observations, CFC-11, Δ^{14}C and T (Figure 4, shown as an example for ENSEMBLE 1). In general, the observations are contained by the model ensemble spread, except for T in the deep ocean, which is too cold in the model.

3.2. Uncertainty of the Statistical Inversion

[30] The inversion method uses the information contained in the tracers to estimate the model parameter K_{bg}, taking into account uncertainties in u_K_{SO}. Key improvements compared to *Schmittner et al.* [2009] are (1) the estimation of the cross-correlation terms; (2) a more refined representation of structured biases in the Likelihood function; and (3) the consideration of the effects of the structural uncertainty (specifically about the implementation of mixing in the SO). Here we demonstrate how these improvements affect the joint posterior pdf of the model parameters. We test the sensitivity of the method to the choice of the statistical (or nuisance) parameters for the distribution of K_{bg}. In this sensitivity test, we do not account for uncertainties in the parameter u_K_{SO}. Therefore, we only use outputs from ENSEMBLE 1.

[31] For illustration, we use two tracers, Δ^{14}C and T, as input for the statistical inversion. We calculate four inversion, which vary the number of statistical parameters to be estimated. The structure of the errors differs from each other by the representation of two main parameters, the bias and the cross correlation of the residuals between the model and the observations. The bias term represents our guess of the mean function of the residuals. We demonstrate the trade-off between complexity of the bias-correction and the covariance structure of the residuals in this simple sensitivity study.

[32] Specifically, we analyze four different assumptions about the structural error terms. First, we use a simple case where the bias is constant and there is no residuals cross correlation; second, we use a constant bias and estimate the cross correlation; third we estimate a linear bias but no residual cross correlation; and fourth, in which linear bias and cross correlation are both estimated. To summarize the experiments in the sensitivity study, we have (1) $\mu = b$, $\rho = 0$, (2) $\mu = b$, $\rho = \hat{\rho}$, (3) $\mu = az + b$, $\rho = 0$, and (4) $\mu = az + b$, $\rho = \hat{\rho}$. Note that the calibration also estimates standard deviation, correlation length and the model parameter, as described in section 2.3. Comparing all pdfs (Figure 5) we see that for the individual pdfs the representation of the bias term can be essential for the model parameter estimation. When a more simplified bias ($\mu = b$) is applied (Figures 5a and 5b), the pdfs in this example are displaced toward higher K_{bg} values, and centered on 0.3 and 0.4 cm^2 s^{-1}. In contrast, with the linear bias estimations, the mode of K_{bg} pdf is centered around 0.15 and 0.2 cm^2 s^{-1}. For the cases with linear bias (Cases c and d), the standard deviation of the residuals of both tracers (Table 1) decrease in comparison to the constant biases cases (Cases a and b). On the other hand, the standard deviations of the residuals are not influenced by the addition of cross-correlation parameters.

[33] The inclusion of the cross-correlation parameter impacts the position of the joint posterior (black curves), and its strength is closely related to the representation of the bias. When the bias has a better representation, which is the linear bias case here (Figures 5c and 5d), the cross-correlation term has little influence on the joint pdf. A comparison of the strength of the cross-correlation parameters (Cases b and d in Table 1) shows that $\rho = 0.70$ when μ is constant, and is much smaller $\rho = 0.40$ when μ is linear. Comparing the posteriors of the Cases a and b (Figures 5a and 5b), ρ can visibly change the posterior when the mean function is less structured. Case b shows a counterintuitive result where the posterior mode is distant from the modes of the individual components (Figure 5b). This result indicates that with a relatively poor representation of the mean (bias) function, considering or neglecting the effects of this residual cross-correlation can drastically change the K_{bg} posterior estimate. This effect becomes less pronounced, as the representation of the model bias term improves (e.g., Figure 5b versus Figure 5c). As discussed by *Cressie* [1993] (pp. 25), "What is one person's (spatial) covariance structure may be another person's mean structure." In other words, there is a trade-off between estimating a mean function for the tracer residuals to account for structural model errors and the magnitude of the residual cross correlation across the considered sources of information.

3.3. Estimating the Uncertainty of Vertical Diffusivity

[34] The analysis so far illustrates how different tracers observations can be combined to reduce uncertainty about one mixing parameter (K_{bg}). This reduction in parametric uncertainty results, at least in the framework of the adopted

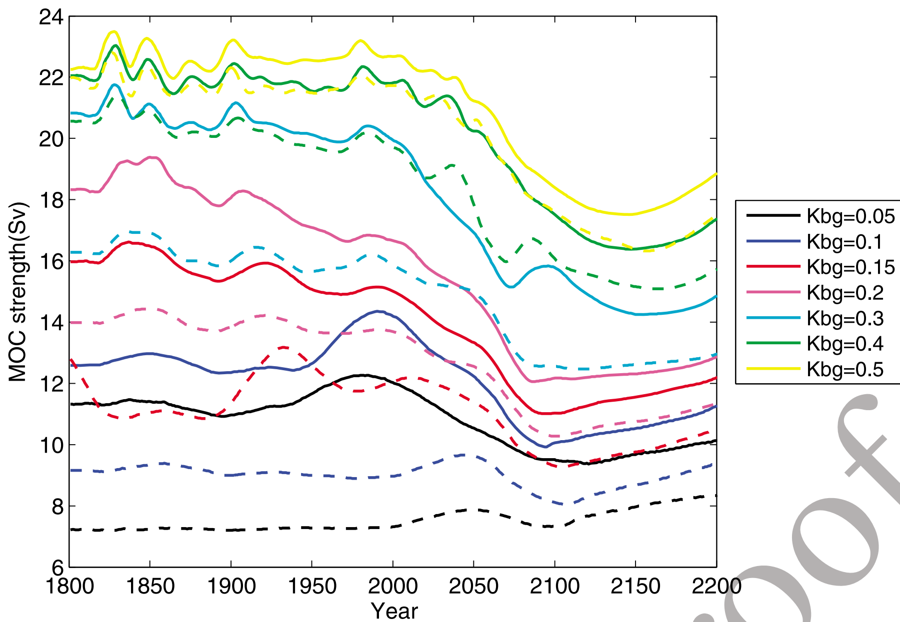

Figure 1. AMOC strength (Sv), defined as the maximum of the transport stream function, from years 1800 to 2200. Dashed lines are for the ENSEMBLE 1 ($u\_K_{SO} = 0$); solid lines are for the ENSEMBLE 2 ($u\_K_{SO} = 1$).

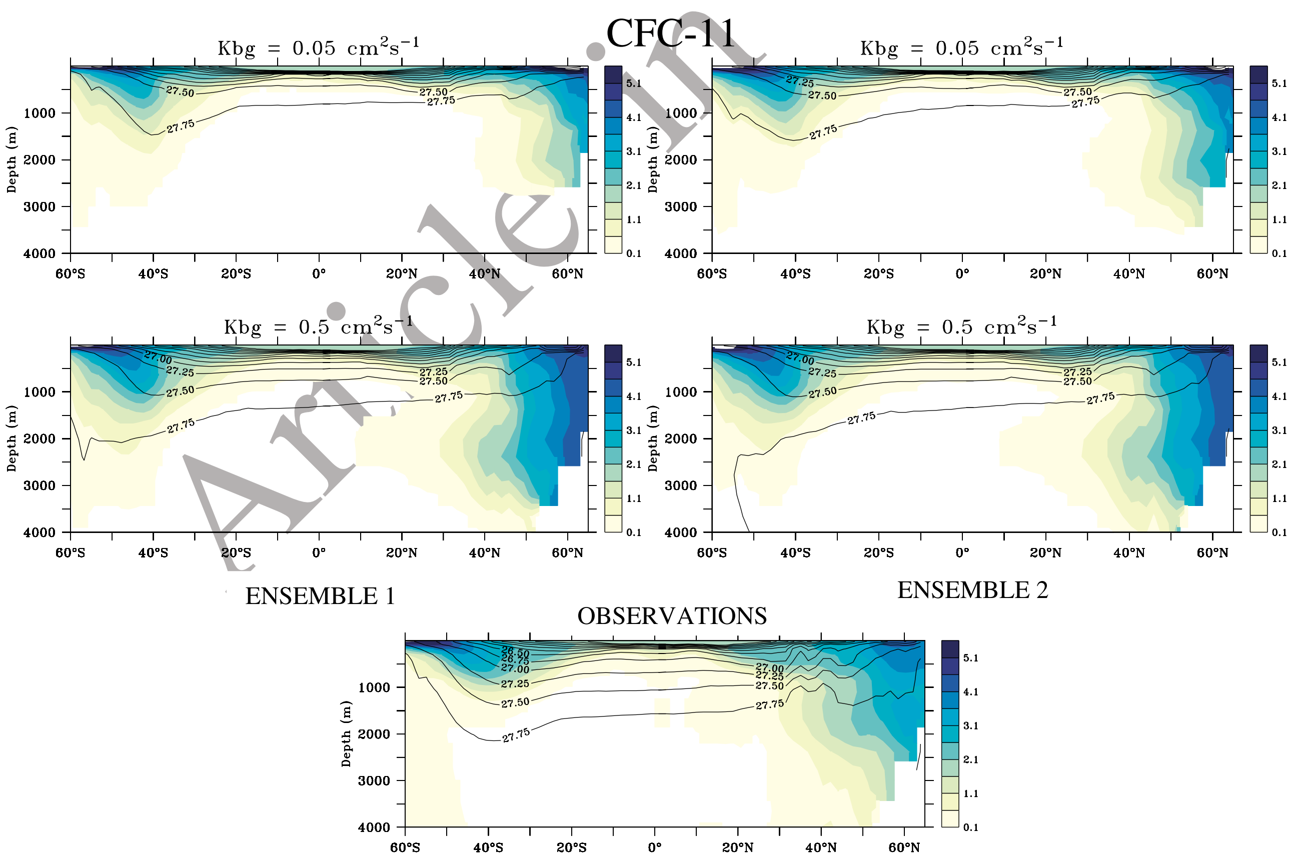

Figure 2. Zonal averages for the Atlantic Ocean of CFC-11 concentration in pmol/kg (color bars) and density anomalies in kg/m^3 (contour lines) for the model with diffusivity of (top) $K_{bg} = 0.05$ and (middle) $K_{bg} = 0.5$. (left) ENSEMBLE 1 ($u\_K_{SO} = 0$) and (right) ENSEMBLE 2 ($u\_K_{SO} = 1$). (bottom) Observations from *Key et al.* [2004] and *Locarnini et al.* [2006].

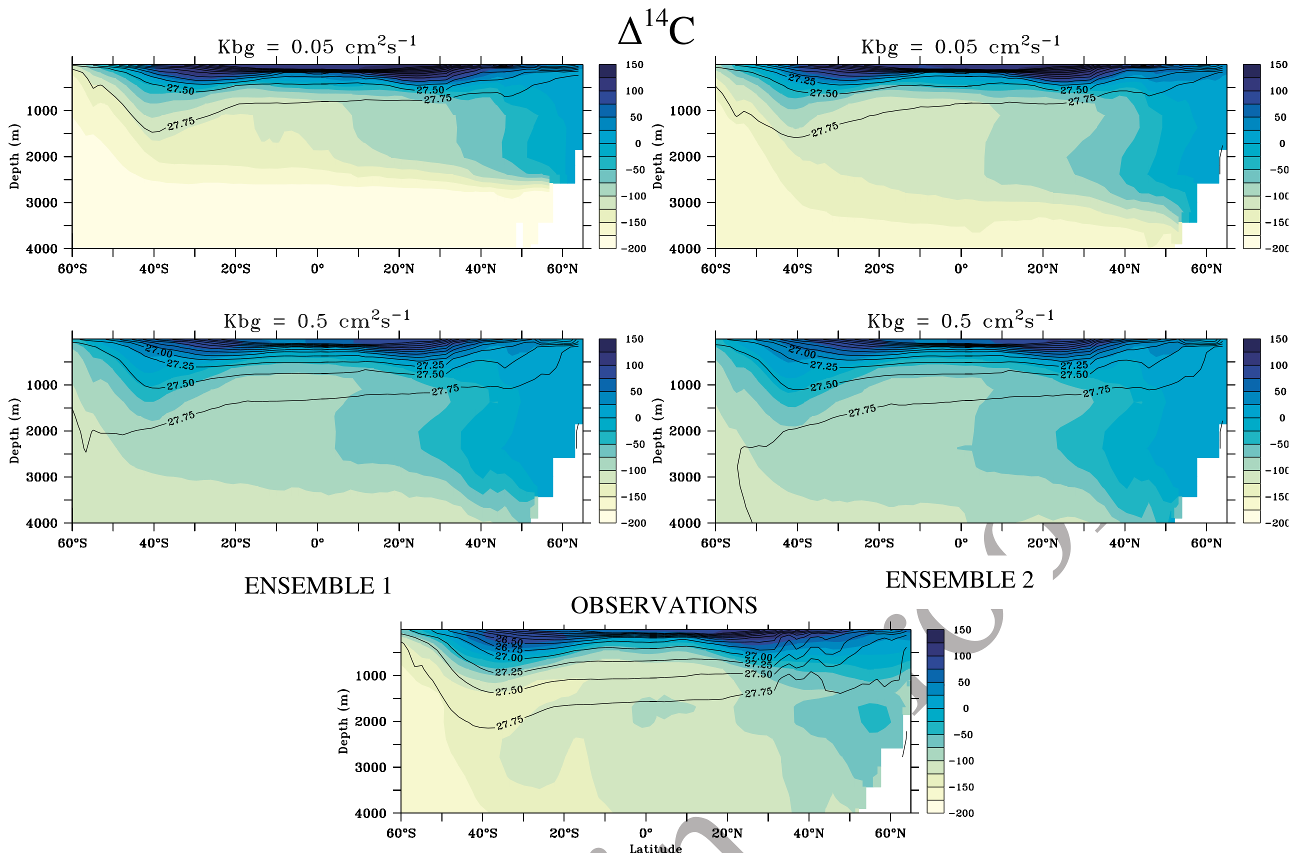

Figure 3. Zonal averages for the Atlantic Ocean of $\Delta^{14}C$ concentration in permil (color bars) and density anomalies in kg/m^3 (contour lines) for the model with diffusivity of (top) $K_{bg} = 0.05$ and (middle) $K_{bg} = 0.5$. (left) ENSEMBLE 1 ($u\_K_{SO} = 0$) and (right) ENSEMBLE 2 ($u\_K_{SO} = 1$). (bottom) Observations from *Key et al.* [2004] and *Locarnini et al.* [2006].

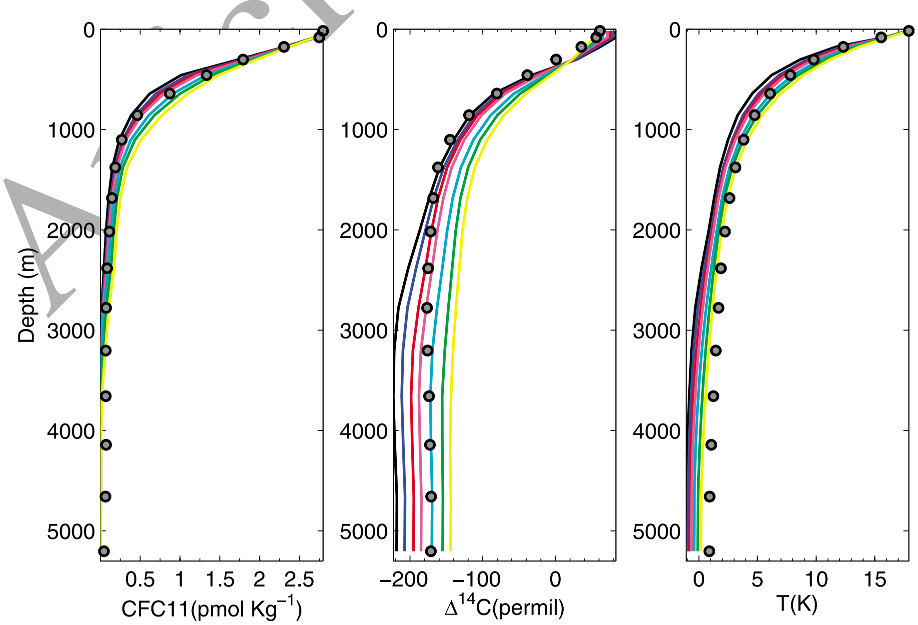

Figure 4. Global averaged profiles of CFC-11 [*Key et al.*, 2004], $\Delta^{14}C$ [*Key et al.*, 2004], and T [*Locarnini et al.*, 2006] for the observations (gray dots) and model ENSEMBLE 1 (colored lines). The legend for the model K_{bg} values is the same as in Figure 1.

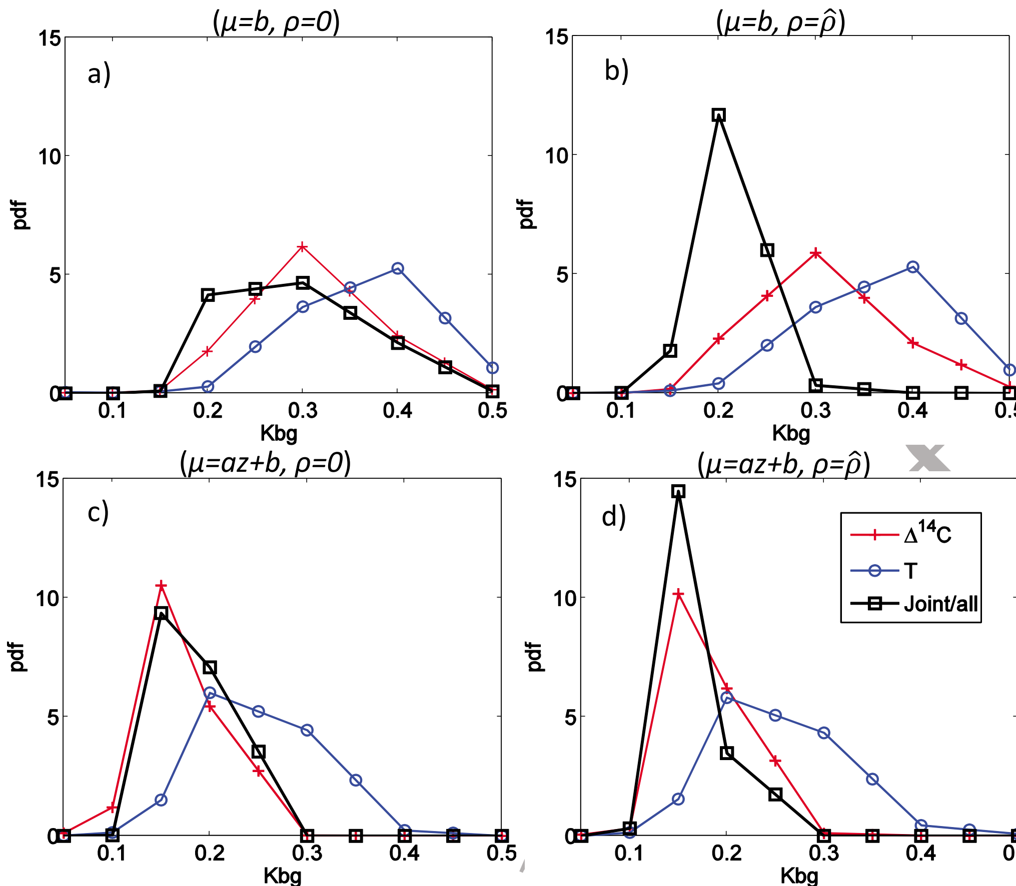

Figure 5. Sensitivity of the model parameter estimation to different treatments of structural model errors. Shown are the posterior probability density function of Δ^{14}C (red lines with crosses) and T (blue lines with circles), and the joint posterior using both observations (black line with squares). The frames are for the cases discussed in the text: (a) [$\mu = b$, $\rho = 0$], (b) [$\mu = b$, $\rho = \hat{\rho}$], (c) [$\mu = az + b$, $\rho = 0$], and (d) [$\mu = az + b$, $\rho = \hat{\rho}$].

model, in a reduction of the prediction uncertainty about the AMOC. Of course, there are several caveats associated with structural errors and other neglected uncertainties in this study. We return to this issue in section 4. In this section we illustrate how this information can potentially be used to reduce uncertainties in two model parameters and improve model hindcasts and projections of the AMOC. Here the inversion uses our best estimate of the model bias term (linear), and accounts for cross-tracer correlation. We make three inversions (Figure 6), one to estimate K_{bg} for the ENSEMBLE 1, a second to estimate K_{bg} for the ENSEMBLE 2, and a third inversion which uses information from both ensembles to generate probability distributions for K_{bg} and u_K_{SO} in a Bayesian model average fashion.

[35] Information from the three considered tracers, CFC-11, T and Δ^{14}C, is introduced in the statistical inversion for the estimation of uncertainties in the model parameters. For comparison, we also show in Figure 6 the K_{bg} pdf obtained using the climatological AMOC observations. The K_{bg} pdf is derived from estimate of the climatological AMOC strength of *Lumpkin and Speer* [2003] by assimilating a single data point assuming a normally distributed error. In principle, the model could be calibrated with both the ocean tracers and AMOC strength data by using the derived

Table 1. Properties of the Statistical Distributions of the Sensitivity Test for the Best K_{bg}[a]

Experiment	Mode ($cm^2\ s^{-1}$) Δ^{14}C	Mode T	Bias (a,b) Δ^{14}C	Bias (a,b) T	σ Δ^{14}C	σ T	Cross Correlation at Best K_{bg}	Mode of Posterior
Case a	0.3	0.4	(−14.0,0)	(0.45,0)	12.5	0.6	–	0.3
Case b	0.3	0.4	(−14.0,0)	(0.45,0)	12.5	0.6	0.70	0.2
Case c	0.15	0.2	(−16.1,9e-3)	(0.22,3.3e-4)	7.7	0.28	–	0.15
Case d	0.15	0.2	(−16.1,9e-3)	(0.22,3.2e-4)	7.7	0.28	0.40	0.15

[a]Mode, bias ($\mu = az + b$), standard deviation, and cross-correlation of residuals for Δ^{14}C and T and mode of the posterior (joint distribution considering all tracers information).

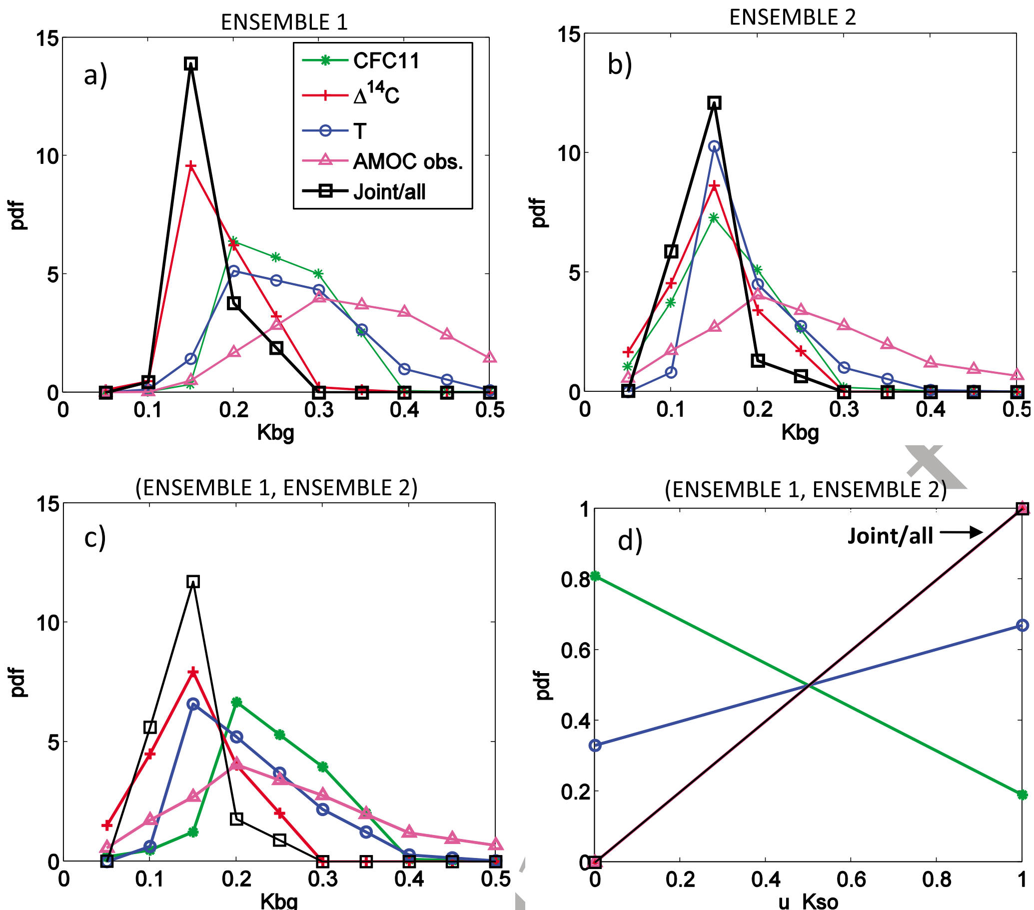

Figure 6. Posterior probability density function of the model parameters for all considered sources of information, the joint posterior using all available information from observations (black line with squares). The climatological AMOC estimate of *Lumpkin and Speer* [2003] is plotted for comparison (pink line with triangles). The K_{bg} estimates are for (a) ENSEMBLE 1, (b) ENSEMBLE 2, (c) ENSEMBLE 1 and ENSEMBLE 2, and (d) the u_K_{SO} estimate is for ENSEMBLE 1 and ENSEMBLE 2.

AMOC pdf as a prior for K_{bg}. However, this would neglect potential correlations between ocean tracer and AMOC strength residual errors. As a proper treatment of AMOC/tracer correlations is beyond the scope of this work, we present the AMOC-derived pdf just for comparison, without assimilating it in the joint posterior pdf.

[36] The tracers distributions of both ensembles show similar behavior. Nevertheless, the ENSEMBLE 1 (Figure 6a) has in general higher K_{bg} modes in comparison to ENSEMBLE 2 (Figure 6b). This result shows that the additional mixing over the upper Southern Ocean increases the overall magnitude of K_v, without changing K_{bg}, and tends to intensify the AMOC. The posterior pdf for K_{bg}, obtained by assimilating observations of the AMOC strength only (lines with triangles), is also displaced to lower values in ENSEMBLE 2, because ENSEMBLE 2 has stronger AMOC values for the same K_{bg} (Figure 1).

[37] When information from both ensembles are added together (Figures 6c and 6d), the ENSEMBLE 2 dominates the Markov chain for Δ^{14}C and T, with probabilities of 100% and 65% for ENSEMBLE 2, respectively. Conversely, CFC-11 has 80% probability of happening ENSEMBLE 1 (Figure 6d). The joint posterior of all tracers encompassing the two ensembles (Figure 6c) is entirely described by ENSEMBLE 2; therefore, the posteriors in Figures 6b and 6c are practically identical.

[38] When all the two model parameters are assimilated jointly (Figure 6c), the considered sources of information have rather different skill in improving K_{bg} estimates and AMOC predictions (see Table 2 for the properties of the statistical distributions). Δ^{14}C has the highest information content with respect to improving K_{bg} estimates, its posterior 95% credible interval (CI) is the tightest (0.21 cm^2 s^{-1}) in comparison to the other tracers. CFC-11 comes in second, with a 95% CI of 0.24 cm^2 s^{-1}, and T comes last with the largest CI of 0.26 cm^2 s^{-1}.

[39] Combining the information of the three considered tracers (line with squares in Figure 6c), favors K_{bg} values in the lower part of the considered range, from 0.1 to 0.2 cm^2 s^{-1}. Note that the joined probability density function is narrower than each individual pdf indicating an advantage of using multiple tracer observations in reducing the parameter uncertainty.

[40] As discussed in previous studies [e.g., *Schmittner et al.* 2009], the K_{bg} value in a coarse resolution ocean model represents the effects of background diffusivity combined

Table 2. Properties of the Statistical Distributions of K_{bg} (Figure 6c) for Each Considered Sources of Information, the Posterior (Joint Distribution Considering All Tracers Information), and the Climatological AMOC Estimate[a]

Observation	Mode	Mean	95% CI	Cross Correlation at Best K_{bg}: Δ^{14}C	CFC-11	T
Δ^{14}C	0.15	0.15	0.22	1	0.06	0.38
CFC-11	0.20	0.23	0.26	–	1	0.02
T	0.15	0.18	0.26	–	–	1
Posterior	0.15	0.16	0.17	–	–	–
Climatological sAMOC	0.20	0.20	0.42	–	–	–

[a]Mode, mean, and 95% credible interval (CI, in cm^2 s^{-1}). Climatological AMOC estimate from *Lumpkin and Speer* [2003]. Also shown are the cross-tracer correlation at the best K_{bg} value estimated in the joint posterior.

with subgridscale diffusivity (i.e., a model shortcoming). Another shortcoming for coarse *z* coordinate ocean models is the numerical diffusivity (Veronis effect), which can generate spurious diapycnal diffusion, especially in long climate simulations, in western boundary regions and regions where the isoneutral slope is large [*Griffies et al.*, 1998, 2000]. Hence, even if our model-based estimate does not represent directly the observational estimate of pelagic diffusivity of 0.1 cm^2 s^{-1} [*Ledwell et al.*, 1993], they appear to be more consistent when we improve on the parameterization of regional mixing in the model.

3.4. AMOC Projections

[41] The joint posterior K_{bg} and u_K_{SO} estimates (Figures 6c and 6d) can be used to derive model projections of the AMOC in 2100 and 2200 (Figure 7). The model hindcast for the maximum AMOC strength in 2000 is about 15–15.5 Sv. In 2100, the expected strength for the AMOC in this model is about 11 Sv. In 2200 the AMOC shows a slight strengthening relative to the 2100 conditions with an expected value of roughly 12 Sv.

[42] The K_{bg} and u_K_{SO} estimates suggest an AMOC hindcast for the year 2000 (Figure 7) that is about 2 Sv weaker than the climatological AMOC estimates of *Lumpkin and Speer* [2003]. The inclusion of the parameter u_K_{SO} in the analysis reduces significantly the discrepancy of the AMOC estimates relative to the K_{bg} (Figure 6c). Other systematic model bias(es), such as too weak buoyancy forcing (e.g., from errors in the simulation of the atmospheric hydrological cycle and surface freshwater fluxes) can compromise the estimates of the current and projected AMOC strength for the Uvic model. Further discussion and implications are described in section 4.

4. Caveats

[43] Our results are subject to many caveats. These caveats point to potentially fruitful research directions. In the statistical part, we consider only highly aggregated data. Basin-wide zonal averages could, for example, provide potentially useful information on where the model performs better. In the projection part, other model parameters, such as those affecting the response of the ocean-atmosphere coupled system, for example, the hydrological cycle [*Saenko and Weaver*, 2004], climate sensitivity or sensitivity of climate to aerosol concentrations, [cf. *Tomassini et al.*, 2007; *Forest et al.*, 2002], are also highly uncertain, and can impact (probably widen) probabilistic AMOC projections and should be considered. In addition, the atmospheric model in UVic is rather simplified, and neglects important ocean-atmosphere feedbacks.

[44] UVic does not use flux correction. Freshwater flux correction is known to improve the salinity and stratification in ocean models [*Sorensen et al.*, 2001], and can be used to improve projections and hindcasts.

[45] In the hindcasts part, other parameters linked to both diapycnal and isopycnal mixing may affect the structure of the AMOC. Nevertheless, according to *Jayne* [2009], tidal mixing parameters in the [*St. Laurent et al.*, 2002] parameterization have relatively low impact on the strength of the AMOC, and that upper-ocean wind-driven mixing may have a much stronger impact.

[46] We show how including regional aspects of vertical mixing can improve the representation of the AMOC. The model parameters uncertainties need to be estimated together as performed here, since addition of new parameters can change the structure of the other calibrations. *Jayne* [2009] describes, "this is the typical conundrum: it is difficult to assess whether any of the given parameterizations improve the model since comparing to observational metrics may obscure compensating errors in different parameterizations."

5. Conclusion

[47] We develop and apply a computationally efficient and statistically sound method to rank and quantify the skill of different sources of information to reduce the uncertainty about ocean model parameters and the resulting climate predictions. We improve on previous work by (1) refining the estimation of errors in the model structure, (2) including several ocean tracers and two model parameters at once in a computationally efficient fashion, and (3) quantifying and ranking the skill of different sources of information to

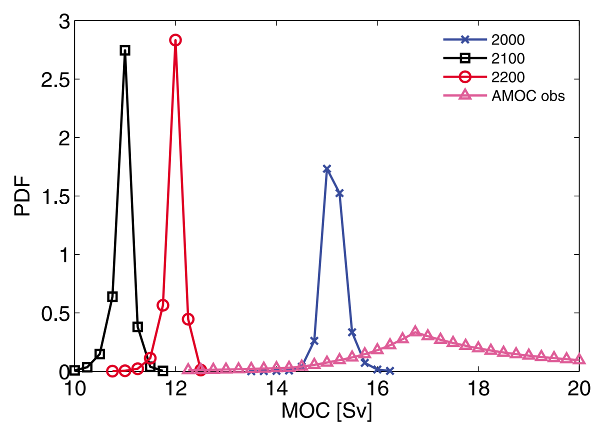

Figure 7. Joint posterior probability density function of model projections of the maximum AMOC strength in the years 2000, 2100, and 2200 using information from the Δ^{14}C, CFC-11, and T observations. The climatological AMOC estimate of *Lumpkin and Speer* [2003] is added for comparison (pink line with triangles).

reduce the uncertainty about a model parameter. Subject to the aforementioned caveats, we show how $\Delta^{14}C$, CFC-11, and T together sharpen the estimates of K_{bg} by 40% and improve AMOC projections in the UVic model.

[48] The K_{bg} derived from individual observations (i.e., $\Delta^{14}C$, CFC-11, T) are broadly consistent, but show slight discrepancies that we attribute predominantly to structural model errors. Of the considered observations, $\Delta^{14}C$ has the highest skill in reducing uncertainties in AMOC projections, but it is also the most distant from the pdf observational derived AMOC estimates. $\Delta^{14}C$ is followed (in decreasing skill of being able to reduce K_{bg} uncertainty) by CFC-11 and T. The second parameter analyzed in this work, u_K_{SO} improved the representations of C14 and T in the model, and improves the representation of the AMOC strength.

[49] AMOC projections show a reduction of the maximum of the joint posterior in 2100 by roughly 25% (3.5 Sv). Perhaps both surprisingly and encouraging, the pdfs of K_{bg} estimated in this study are quite similar among the considered ocean tracers and the two ensembles analyzed, which have different representations of the upper Southern Oceanmixing and AMOC. This convergence of K_{bg} estimates based on different sources of information and parameterizations suggest that K_{bg} can be robustly estimated from the oceanic tracers studied here.

[50] **Acknowledgments.** We thank Mike Eby, Damon Matthews, Bob Key, and Ray Najjar for helpful discussions and feedback. This work is partially supported by the National Science Foundation as well as by the U.S. Department of Energy's Office of Science (BER) through the Northeastern Regional Center of the National Institute for Climatic Change Research. This work was partially supported by the U.S. Geological Survey. Any errors and opinions are those of the authors alone.

References

Baehr, J., D. McInerney, K. Keller, and J. Marotzke (2008), Optimization of an observing system design for the North Atlantic Meridional Overturning Circulation, *J. Atmos. Oceanic Technol.*, *25*, 625–634.

Barnard, J., R. McCulloch, and X. Meng (2000), Modeling covariance matrices in terms of standard deviations and correlations with application to shrinkage, *Stat. Sinica*, *10*, 1281–1311.

Bhat, K. S., M. Haran, R. Tonkonojenkov, and K. Keller (2009), Inferring likelihoods and climate system characteristics from climate models and multiple tracers, technical report, Dep. of Stat., Penn. State Univ., University Park, Pa.

Broecker, W. S., and T. H. Peng (1987), Gas exchange rates between air and sea, *Tellus*, *26*, 21–35.

Bryan, K., and L. J. Lewis (1979), A water mass model of the world ocean, *J. Geophys. Res.*, *84*(C5), 2503–2517, doi:10.1029/JC084iC05p02503.

Cressie, N. A. (1993), *Statistics for Spatial Data*, 900 pp., Wiley, New York.

Doney, S. C., et al. (2004), Evaluating global ocean carbon models: The importance of realistic physics, *Global Biogeochem. Cycles*, *18*, GB3017, doi:10.1029/2003GB002150.

England, M. H. (1993), Representing the global scale water masses in ocean general circulation models, *J. Phys. Oceanogr.*, *23*, 1523–1552.

Ferrari, R., J. C. McWilliams, V. M. Canuto, and M. Dubovikov (2008), Parameterization of eddy fluxes near oceanic boundaries, *J. Clim.*, *21*, 2770–2789, doi:10.1175/2007JCLI1510.1.

Forest, C. E., P. H. Stone, A. P. Sokolov, M. R. Allen, and M. D. Webster (2002), Quantifying uncertainties in climate system properties with the use of recent climate observations, *Science*, *295*, 113–117, doi:10.1126/science.1064419.

Gao, Y., H. Drange, and M. Bentsen (2003), Effects of diapycnal and isopycnal mixing on the ventilation of CFCs in the North Atlantic in an isopycnic coordinate OGCM, *Tellus Ser. B*, *55*, 837–854.

Gelman, A., J. B. Carlin, H. S. Stern, and D. B. Rubin (2003), *Bayesian Data Analysis*, 2nd ed., CRC Press, London.

Gent, P. R., and J. C. McWilliams (1990), Isopycnal mixing in ocean circulation models, *J. Phys. Oceanogr.*, *20*, 150–155.

Gnanadesikan, A. (1999), A simple predictive model for the structure of the oceanic pycnocline, *Science*, *283*, 2077–2079.

Griffies, S. M., A. Gnanadesikan, R. C. Pacanowski, V. D. Larichev, J. K. Dukowicz, and R. D. Smith (1998), Isoneutral diffusion in a *z* coordinate ocean model, *J. Phys. Oceanogr.*, *28*, 805–830.

Griffies, S. M., R. C. Pacanowski, and R. W. Hallberg (2000), Spurious diapycnal mixing associated with advection in a z-coordinate ocean model, *Mon. Weather Rev.*, *128*(3), 538–564.

Hansen, J., and M. Sato (2004), Greenhouse gas growth rates, *Proc. Natl. Acad. Sci. U.S.A.*, *101*, 16,109–16,114.

Ito, T., J. Marshall, and M. Follows (2004), What controls the uptake of transient tracers in the Southern Ocean?, *Global Biogeochem. Cycles*, *18*, GB2021, doi:10.1029/2003GB002103.

Jayne, S. R. (2009), The impact of abyssal mixing parameterizations in an ocean general circulation model, *J. Phys. Oceanogr.*, *39*, 1756–1775.

Keller, K., K. Tan, F. M. M. Morel, and D. F. Bradford (2000), Preserving the ocean circulation: Implications for climate policy, *Clim. Change*, *47*, 17–43.

Keller, K., C. Deutsch, M. G. Hall, and D. F. Bradford (2007), Early detection of changes in the North Atlantic Meridional Overturning Circulation: Implications for the design of ocean observation systems, *J. Clim.*, *20*, 145–157.

Key, R. M., A. Kozyr, C. L. Sabine, K. Lee, R. Wanninkhof, J. Bullister, R. A. Feely, F. Millero, C. Mordy, and T.-H. Peng (2004), A global ocean carbon climatology: Results from Global Data Analysis Project (GLODAP), *Global Biogeochem. Cycles*, *18*, GB4031, doi:10.1029/2004GB002247.

Koch, D., D. Jacob, I. Tegen, D. Rind, and M. Chin (1999), Tropospheric sulfur simulation and sulfate direct radiative forcing in the Goddard Institute for Space Studies general circulation model, *J. Geophys. Res.*, *104*(D19), 23,799–23,822, doi:10.1029/1999JD900248.

Large, W. G., J. C. McWilliams, and S. C. Doney (2004), Oceanic vertical mixing: A review and a model with nonlocal boundary layer parameterisation, *Rev. Geophys.*, *32*, 363–403.

Ledwell, J. R., A. J. Watson, and C. S. Law (1993), Evidence for slow mixing across the pycnocline from an open-ocean tracer-release experiment, *Nature*, *364*, 701–703.

Locarnini, R. A., A. V. Mishonov, J. Antonov, T. Boyer, and H. E. Garcia (2006), *World Ocean Atlas 2005*, vol. 1, *Temperature*, *NOAA Atlas NESDIS*, vol. 61, 182 pp., NOAA, Silver Spring, Md.

Lu, N., and D. L. Zimmerman (2005), The likelihood ratio test for a separable covariance matrix, *Stat. Prob. Lett.*, *73*(4), 449–457.

Lumpkin, R., and K. Speer (2003), Large-scale vertical and horizontal circulation in the North Atlantic Ocean, *J. Phys. Oceanogr.*, *33*, 1902–1920.

Marotzke, J. (1997), Boundary mixing and the dynamics of three-dimensional thermohaline circulation, *J. Phys. Oceanogr.*, *27*, 1713–1728.

McManus, J. F., R. Francois, J. M. Gherardi, L. D. Keigwin, and S. Brown-Leger (2004), Collapse and rapid resumption of Atlantic meridional circulation linked to deglacial climate changes, *Nature*, *428*, 834–837.

Meehl, G. H., et al. (2007), Global climate projections, in *Climate Change 2007: The Physical Science Basis: Contribution of Working Group I to the Fourth Assessment Report of the Intergovernmental Panel on Climate Change*, edited by S. Solomon et al., pp. 747–846, Cambridge Univ. Press, Cambridge, U. K.

Metropolis, N., A. W. Rosenbluth, M. N. Rosenbluth, A. H. Teller, and E. Teller (1953), Equation of state calculations by fast computing machines, *J. Chem. Phys.*, *21*, 1087–1092.

Moum, J. N., and W. D. Smyth (2001), Upper ocean mixing processes, in *Encyclopedia of Ocean Sciences*, edited by J. H. Steele, K. K. Turekian, and S. A. Thorpe, pp. 3093–3100, Academic, New York.

Munk, W., and C. Wunsch (1998), Abyssal recipes: Part II. Energetics of tidal and wind mixing, *Deep Sea Res. Part I*, *13*, 1977–2010.

Naveira Garabato, A. C., K. L. Polzin, B. A. King, K. J. Heywood, and M. Visbeck (2004), Widespread intense turbulent mixing in the Southern Ocean, *Science*, *303*, 210–213.

Pacanowski, R., and S. G. H. Philander (1981), Parameterization of vertical mixing in numerical models of tropical oceans, *J. Phys. Oceanogr.*, *11*, 1443–1451.

Pacanowski, R. C. (1995), MOM 2 documentation: Users guide and reference manual, ver. 1.0, *Ocean Group Tech. Rep. 3*, Geophys. Fluid Dyn. Lab., Princeton, N. J.

Patwardhan, A., et al. (2007), Assessing key vulnerabilities and the risk from climate change, in *Climate Change 2007: Impacts, Adaptation and Vulnerability: Contribution of Working Group II to the Fourth Assessment Report of the Intergovernmental Panel on Climate Change*, edited by M. L. Parry et al., chap. 19, pp. 779–810, Cambridge Univ. Press, Cambridge, U. K.

Saenko, O. A., and A. J. Weaver (2004), What drives heat transport in the Atlantic: Sensitivity to mechanical energy supply and buoyancy forcing in the Southern Ocean, *Geophys. Res. Lett.*, *31*, L20305, doi:10.1029/2004GL020671.

Sato, M., J. E. Hansen, M. P. McCormick, and J. B. Pollack (1993), Stratospheric aerosol optical depth, 1850–1990, *J. Geophys. Res.*, *98*(D12), 22,987–22,994, doi:10.1029/93JD02553.

Schmittner, A., and A. J. Weaver (2001), Dependence of multiple climate states on ocean mixing parameters, *Geophys. Res. Lett.*, *28*(6), 1027–1030, doi:10.1029/2000GL012410.

Schmittner, A., A. Oschlies, X. Giraud, M. Eby, and H. L. Simmons (2005), A global model of the marine ecosystem for long-term simulations: Sensitivity to ocean mixing, buoyancy forcing, particle sinking, and dissolved organic matter cycling, *Global Biogeochem. Cycles*, *19*, GB3004, doi:10.1029/2004GB002283.

Schmittner, A., N. M. Urban, K. Keller, and D. Matthews (2009), Using tracer observations to reduce the uncertainty of ocean diapycnal mixing and climate carbon-cycle projections, *Global Biogeochem. Cycles*, *23*, GB4009, doi:10.1029/2008GB003421.

Simmons, H. L., S. Jayne, L. St. Laurent, and A. Weaver (2004), Tidally driven mixing in a numerical model of the ocean general circulation, *Ocean Modell.*, *6*, 245–263, doi:10.1016/S1463-5003(03)00011-8.

Smyth, W. D., and J. N. Moum (2001), Three-dimensional turbulence, in *Encyclopedia of Ocean Sciences*, edited by J. H. Steele, K. K. Turekian, and S. A. Thorpe, pp. 18–25, Academic, London.

Sokolov, A., C. Wang, G. Holian, P. Stone, and R. Prinn (1998), Uncertainty in the oceanic heat and carbon uptake and its impact on climate projections, *Geophys. Res. Lett.*, *25*(19), 3603–3606, doi:10.1029/98GL02696.

Sorensen, J., J. Ribbe, and G. Shaffer (2001), Antarctic intermediate water mass formation in ocean general circulation models, *J. Phys. Oceanogr.*, *31*, 3295–3311.

Sriver, R. L., M. Goes, M. E. Mann, and K. Keller (2010), Climate response to tropical cyclone-induced ocean mixing in an Earth system model of intermediate complexity, *J. Geophys. Res.*, doi:10.1029/2010JC006106, in press.

Stein, M. L. (1999), *Interpolation of Spatial Data: Some Theory for Kriging*, 247 pp., Springer, New York.

St. Laurent, L., H. L. Simmons, and S. R. Jayne (2002), Estimating tidally driven mixing in the deep ocean, *Geophys. Res. Lett.*, *29*(23), 2106, doi:10.1029/2002GL015633.

Stuiver, M., and H. A Polach (1977), Discussion: Reporting of ^{14}C data, *Radiocarbon*, *19*(3), 355–363.

Toggweiler, J. R., K. Dixon, and K. Bryan (1989), Simulations of radiocarbon in a coarse-resolution, world ocean model: 2. Distributions of bomb-produced ^{14}C, *J. Geophys. Res.*, *94*(C6), 8243–8264, doi:10.1029/JC094iC06p08243.

Tomassini, L., P. Reichert, R. Knutti, T. F. Stocker, and M. Borsuk (2007), Robust Bayesian uncertainty analysis of climate system properties using Markov chain Monte Carlo methods, *J. Clim.*, *20*, 1239–1254.

Weaver, A. J., et al. (2001), The UVic Earth system climate model: Model description, climatology, and applications to past, present and future climates, *Atmos. Ocean*, *39*(4), 361–428.

Wunsch, C., and R. Ferrari (2004), Vertical mixing, energy, and the general circulation of the oceans, *Ann. Rev. Fluid Mech.*, *36*, 281–314.

Zickfeld, K., A. Levermann, M. Morgan, T. Kuhlbrodt, S. Rahmstorf, and D. Keith (2007), Expert judgements on the response of the Atlantic Meridional Overturning Circulation to climate change, *Clim. Change*, *82*, 235–265.

Zickfeld, K., M. Eby, and A. J. Weaver (2008), Carbon cycle feedbacks of changes in the Atlantic Meridional Overturning Circulation under future atmospheric CO_2, *Global Biogeochem. Cycles*, *22*, GB3024, doi:10.1029/2007GB003118.

M. Goes, K. Keller, R. Tonkonojenkov, and N. M. Urban, Department of Geosciences, Pennsylvania State University, University Park, PA 16802, USA. (marlosgoes@hotmail.com)

M. Haran, Department of Statistics, Pennsylvania State University, University Park, PA 16802, USA.

A. Schmittner, College of Oceanic and Atmospheric Sciences, Oregon State University, Corvallis, OR 97331-5503, USA.